ARTIFICIAL NEURAL NETWORK-BASED OPTIMIZATION OF THE CRYOGENIC-INTERNAL DIAMOND BURNISHING PROCESS IN TERMS OF SURFACE QUALITY

Nguyen Van Thai[1], Le Van An[2], Nguyen Trung Thanh[1,*]

DOI: http://doi.org/10.57001/huih5804.2024.180

ABSTRACT

Internal diamond burnishing is a prominent solution to produce surface finishing for interior holes. This work aims to propose a novel diamond burnishing process, in which an integrative lubrication using the Vortex tube and liquid CO_2 is applied. Three key process parameters, including the spindle speed (S), feed rate (f), and burnishing depth (D) are optimized to decrease the surface roughness (SR) and improve the Vickers hardness (VH). The Box-Behnken method is applied to conduct the burnishing experiments. The artificial neural network (ANN) is used to develop burnishing response models, while the entropy method is utilized to compute the weights. The optimal solution is determined using the multiple-objective particle swarm optimization (MOPSO) algorithm. The results indicated that the optimal outcomes of the S, D, and f were 630rpm, 0.12mm, and 0.04mm/rev., respectively. The SR was decreased by 60.9%, while the VH was increased by 10.2% at the optimal solution. The outcomes could be applied to practical diamond burnishing to enhance the surface quality of the internal holes. The optimizing technique could be used to present the non-linear data and obtain optimal global results.

Keywords: *Internal diamond burnishing operation; Surface quality; Artificial neural network; MOPSO; Optimization.*

[1]Faculty of Mechanical Engineering, Le Quy Don Technical University, Vietnam
[2]Faculty of Engineering and Technology, Nguyen Tat Thanh University, Vietnam
[*]Email: trungthanhk21@mta.edu.vn
Received: 20/02/2024
Revised: 05/5/2024
Accepted: 25/5/2024

1. INTRODUCTION

One of the chipless finishing techniques is called "diamond burnishing", in which the workpiece's surface is rubbed by the spherical tip of a tool composed of real diamond, causing plastic deformation. To get better surface integrity properties, the workpiece can be burnished with a diamond wheel. To provide a mirror-like surface quality on ferrous and nonferrous materials, it is a cost-effective and versatile method. Compared to the procedures of grinding, lapping, and polishing, it is more efficient.

Numerous diamond burnishing operations have been examined and refined to enhance diverse technological results. Experimental and FEM tests were performed on the sliding burnishing of AISI 316Ti chromium nickel steel by Maximov et al. to determine the effect of tool tip radius (r) and burnishing force (BF) on the SR, VH, residual stress, fatigue strength, and wear resistance of the machined surfaces [1]. It has been found that this method of machining has a beneficial effect on all the characteristics listed. Similar results were obtained when analyzing the slide burnishing of hourglass-shaped tensile specimens made of 41Cr4 steel [2]. Maximov et al. classified the applied variants as smoothing, deep or mixed burnishing, and they optimized the main process parameters (r, BF) applicable to each variant during the machining of 41Cr4 steel [3]. Based on the results of experiments, Korzynski et al. showed that there are correlations between the three-dimensional roughness parameters in diamond burnishing, so it is sufficient to evaluate some of the roughness parameters when examining the process [4]. Furthermore, correlation equations were determined to estimate some roughness indexes based on the technological parameters for diamond burnishing of 317Ti stainless steel. Kluz et al. used ANN models to estimate the expected value of surface roughness for sliding burnishing of 42CrMo4 heat-treated steel with polycrystalline diamond and cemented carbide tip tools [5]. Sachin et al. presented that the SR of 0.2µm and VH of 397.5 HV for the burnished 17-4 stainless steel could be obtained using the optimal S, f, and BF [6]. Maximov et al. emphasized that the fatigue limit and life of the processed 41Cr4 steel could be improved by 22.7% and 100%, respectively with the support of the diamond burnishing process [2]. Zaghal et al. indicated that a better surface quality of the burnished 42CrMo4 was obtained with the aid of the diamond burnishing, as compare to the grinding operation [7]. A novel simulation model was developed to predict the SR based on FEM approach [8]. The small deviations indicated that the developed model was adequate. The optimal values of the f, BF, and r were selected to decrease the SR and enhance the VH of the burnished

CuAl8Fe3 bronze [9]. The energy efficiency, coefficient and friction, and specific wear rate were enhanced using optimal S, f, D, and r with the genetic algorithm [10]. Maximov et el. presented that the diamond burnishing process generated higher depths of affected layers, leading to larger fatigue strength [11]. However, the diamond burnishing operation under the impacts of the Vortex tube and cryogenic cooling has not been investigated. Moreover, the optimal parameters have not been selected to decrease the SR and improve the VH.

The following section presents the optimization strategy. After that, the experimental setup and conversations are explained. Lastly, some conclusions are made.

2. OPTIMIZATION FRAMEWORK

In the current work, the surface roughness (SR) and Vickers hardness (VH) are considered as important burnishing responses.

The SR is calculated as:

$$SR = \frac{\sum_{i=1}^{n} Ra_i}{n} \quad (1)$$

where Ra_i and n are the average roughness of the i_{th} position and the number of positions, respectively.

The VH is calculated as:

$$VH = \frac{\sum_{i=1}^{n} VH_i}{n} \quad (2)$$

where VH_i and n denote the Vickers hardness of the i_{th} position and the number of positions, respectively.

Three key process parameters, including the spindle speed, feed rate, and burnishing depth are listed as optimization inputs. The other factors, including the flow rate of cryogenic CO2, spraying distance, pitch angle, and air pressure are kept at fixed values. The process parameters and their levels are presented in Table 1. The values of the spindle speed and feed rate are determined based on the characteristics of the lathe. The burnishing depth is determined based on recommendations of the manufacturer of the diamond tool. These values are confirmed with data of the related publications.

Therefore, the optimization issue is defined as below:

Finding X = [S, D, and f].

Maximizing VH; Minimizing SR.

Constraints: 150 ≤ S ≤ 630rpm; 0.05 ≤ D ≤ 0.12mm; 0.04 ≤ f ≤ 0.08mm/rev.

Table 1. Process inputs for the internal diamond burnishing operation

Symbol	Process parameters	Levels
S	Spindle speed (rpm)	105-370-630
D	Burnishing depth (mm)	0.05-0.08-0.12
f	Feed rate (mm/rev)	0.04-0.06-0.08

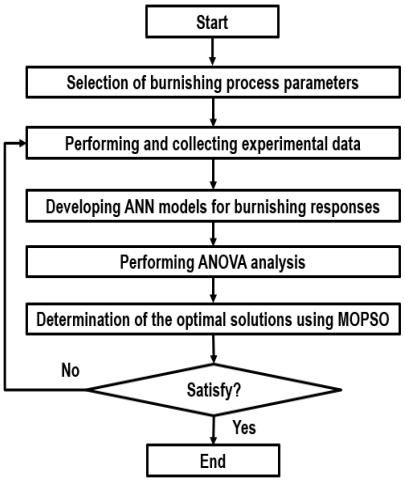

Fig. 1. Optimization approach for the internal diamond burnishing operation

The optimizing procedure for the burnishing process is illustrated in Fig. 1:

Step 1: Executing burnishing experiments using the the Box-Behnken method.

The Box-Behnken method is an effective design of the experiment, in which each factor with three levels (-1, 0, +1) presents the lowest, middle, and highest ranges. The design points are assigned on the center and edge of the block. This approach decreases the number of experiments, leading to reduction in the costs and human efforts. The number of experiments (N) in the Box-Behnken method is calculated as:

$$N = 2m(m-1) + P_C \quad (3)$$

where m and P_C present the number of parameters and the number of center points, respectively. In this work, three process parameters having three levels and five center points are employed; hence, 17 experiments are generated.

Step 2: Developing optimal ANN models of the output objectives are developed regarding burnishing parameters [10].

ANNs are thought of as instruments that can relate a collection of parameters for input and output in various systems. It is a sophisticated information processing system made up of linked segmental processing units known as neurons. These neurons obtained the input data (x_i, x_j, … x_n) from external sources, processed it generally using a non-linear operation, and then produced the final results as an output.

ANNs function in two stages: First, they learn, and then they store that knowledge in connections known as weights (we_i). Each neuron receives inputs attached with a weight. A bias (b_i) can be defined as a type of connection weight with a constant non-zero value added to the summation of weighted inputs ($we_{ij} \times x_j$) forms the input to the transfer function. The summation (u_i) of the input weighted function and bias is given as:

$$u_i = \sum_{j=1}^{N} we_{ij} x_j + b_i \quad (4)$$

Step 3: The weight of each turning response is calculated using the entropy method.

For maximizing aim, the measured response (r_{ij}) is computed as:

$$r_{ij} = \frac{x_{ij}}{\max\limits_{j} x_{ij}}, (i = 1,...,m; j = 1,...,n) \quad (5)$$

For minimizing aim, the measured response (r_{ij}) is computed as:

$$r_{ij} = \frac{\min\limits_{j} x_{ij}}{x_{ij}}, (i = 1,...,m; j = 1,...,n) \quad (6)$$

The normalized response (p_{ij}) are computed as:

$$p_{ij} = \frac{r_{ij}}{\sum\limits_{i=1}^{m} r_{ij}}, (i = 1,...,m; j = 1,...,n) \quad (7)$$

The entropy value (E_j) of the i_{th} index is calculated as:

$$E_j = -\frac{\sum\limits_{j=1}^{m} p_{ij} \times \ln p_{ij}}{\ln m}, (i = 1,...,m; j = 1,...,n) \quad (8)$$

The entropy weight (ω_i) of each response is calculated as:

$$\omega_i = \frac{1 - E_j}{\sum\limits_{j=1}^{n} (1 - E_j)}, \sum_{j=1}^{n} w_j (j = 1,...,n) \quad (9)$$

Step 3: Selection of optimal solution using multiple-objective particle swarm optimization (MOPSO) [11].

A potent optimization method for resolving the trade-off analysis between opposing reactions is the MOPSO. In order to obtain the global optimal solution, the MOPSO algorithm optimizes effectively and efficiently while requiring the least amount of computing time.

In the D-design space, each particle is given a velocity vector V (v_1, v_2,…, v_D) and a position vector X (x_1, x_2, …, x_D). Each particle is associated with its particular best, P_i (p_{i1}, p_{i2},…, p_{id}) which is defined by its own best performance in the swarm. Similarly, an overall best performance of the particle with respect to the swarm defined global best is gbest. Initialized velocity and position vector values are stated as follows:

$$T_{i,d} = (T_d^{max} - T_d^{min}) rand + T_d^{min}, d = 1,...,D; i = 1,2,...,N \quad (10)$$

where T_d^{max} and T_d^{min} presents the maximum and minimum values of i_{th} particle in the d_{th} design space, respectively, while rand denotes the random number in the range (0,1).

The particles move toward the best position based on the bellow equations:

$$v_i^{n+1} = \omega V_i^t + c_1 r_1 (x_{pbest} - X_i^t) + c_2 r_2 (x_{gbest} - X_i^t) \quad (11)$$

$$X_i^{t+1} = X_i^t + V_i^{t+1} \quad (12)$$

where c_1 and c_2 are cognitive acceleration and social acceleration coefficients. ω presents inertia weight. r_1 and r_2 are random numbers in the range (0, 1). x_{pbest} and x_{gbest} are the personal best and global best of the particle. X^t_i and V^t_i are the current position and velocity of the i_{th} particle. The ω is computed as:

$$\omega_n = \omega_{max} - \frac{(\omega_{max} - \omega_{min}) \times n}{it_{max}}, n = 1,2...,it max \quad (13)$$

where ω_{max} and ω_{min} are the maximum and minimum values of the inertia weight. The it_{max} presents the maximum number of iterations.

Table 2. Chemical compositions of the S45C steel

Elements	C	Si	Mn	P	S	Ni	Cr	Cu
%	0.46	0.25	0.75	0.03	0.035	0.2	0.2	0.3

3. EXPERIMENTAL SETTING

The burnishing samples are made of hardened steel labeled S45C steel. The material chosen is selected due to its wide applications in manufacturing components, including gears, shafts, axles, and crane wheels. The chemical compositions of the S45C steel are shown in Table 2. The pre-machining processes, including the drilling and turning, are applied to produce the through-hole in each specimen. The dimensions are the length of 60mm, the internal diameter of 45mm, and the outer diameter of 55mm, respectively. The average roughness and Vicker hardness of the machined surface are approximately 3.68µm and 210.8HV, respectively.

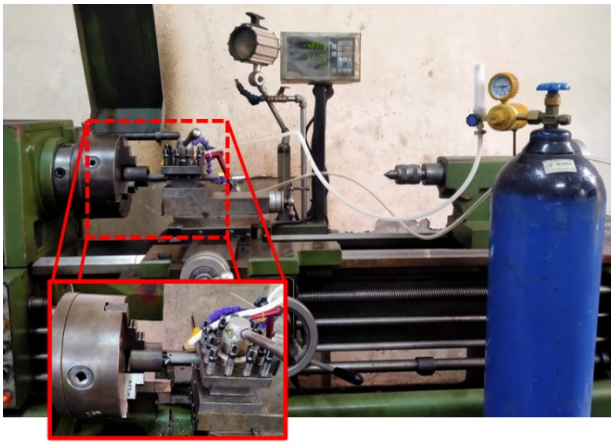

(a) Experimental setting

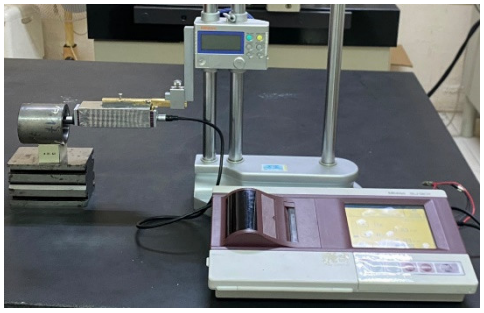

(b) Measuring average roughness

(c) Measuring Vickers hardness

Fig. 2. Experiments of the diamond burnishing operation

The burnishing trails are done with the aid of a conventional lathe (Fig. 2a). The workpiece is positioned and tightly clamped using a jaw-centering chuck. The diamond burnishing tool is clamped to the tool post. The compressed air is supplied to the Vortex tube for generating the cold air. The liquid CO_2 is delivered to the burnishing region by using a straight tube.

Using a tester known as the Mitutoyo Surftest-301, the roughness of the machined surface is assessed in three separate locations by ISO 4287 (Fig. 2b). All machining specimens are measured at 4 mm in length. Wilson Wolpert is the tester used to assess the Vicker hardness at three distinct spots on the burnished surface (Fig. 2c). For every hardness test, a pressing load of 5kG and a dwell period of 15 seconds are employed.

4. RESULTS AND DISCUSSIONS

4.1. Development of ANN models

The experimental results of the burnishing trials are exhibited in Table 3.

Table 3. Experimental data for the internal diamond burnishing operation

No.	S (rpm)	D (mm)	f (mm/rev)	SR (µm)	VH (HV)
1	630	0.05	0.06	0.51	296.2
2	370	0.05	0.08	0.84	292.4
3	370	0.08	0.06	0.44	304.8
4	370	0.08	0.06	0.44	304.9
5	370	0.08	0.06	0.46	304.2
6	370	0.12	0.08	0.54	320.6
7	630	0.08	0.08	0.58	293.4
8	370	0.12	0.04	0.25	336.6
9	630	0.08	0.04	0.31	322.4
10	105	0.05	0.06	0.81	313.5
11	105	0.08	0.04	0.63	329.4
12	630	0.12	0.06	0.28	314.8
13	105	0.12	0.06	0.62	337.2
14	368	0.08	0.06	0.45	304.4
15	105	0.08	0.08	0.86	318.2
16	370	0.08	0.06	0.46	304.4
17	370	0.05	0.04	0.59	317.4

Based on the literature survey, the architecture of the ANN model in most studies has been determined using trial and error. The types of networks, the training function, performance function, transfer function, and learning function are feed forward back propagation, BFGS quasi-Newton, mean squared error, log sigmoid, and gradient descent with momentum weight and bias learning function, respectively. The number of hidden neurons and the number of hidden layers are 20 and 6, respectively (Fig. 3).

Fig. 4 displays the regression graphs of feed forward back propagation models for the test, validation, and training stages. The dependability of the output criteria is presented by the correlation coefficients of the training and testing stages for the generated feed forward back propagation models, which are 0.9882 and 0.9998, respectively.

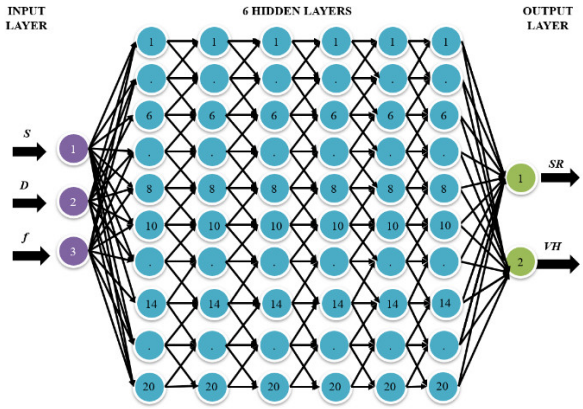

Fig. 3. The architecture of the ANN model

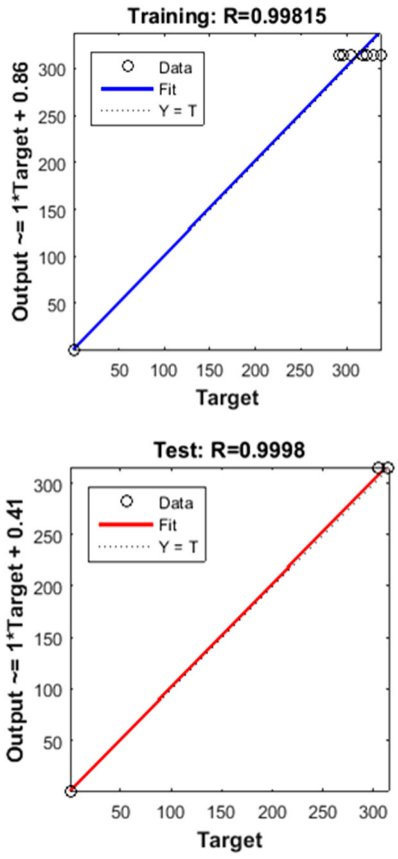

Fig. 4. Regression plots for the ANN model

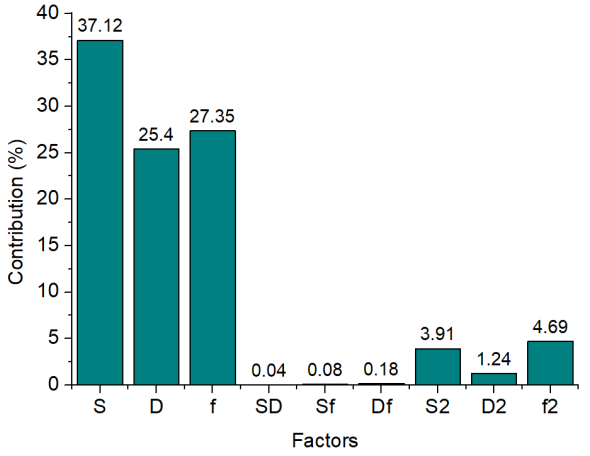

(a) Parameter contributions for the SR model

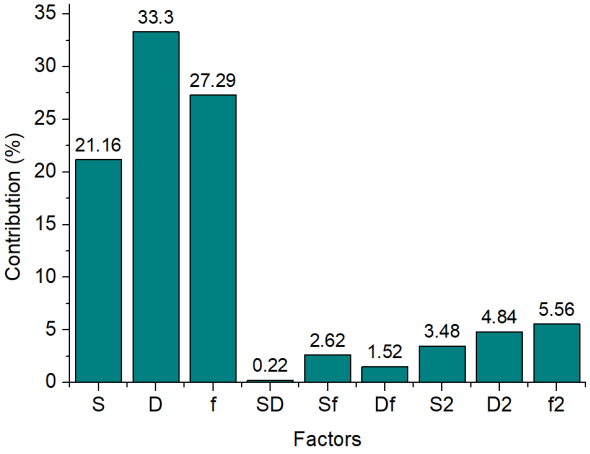

(b) Parameter contributions for the VH model

Fig. 5. Parameter contributions for the burnishing responses

4.2. ANOVA results

ANOVA analysis is applied to find the significant parameters and model adequacy.

Table 4 presents ANOVA results for the SR model. We find that "F value" of the model is 31.33, which confirms that it is significant. The level of significance is 0.05, which is a confidence level of 95%. R^2 of 0.9672 is in reasonable agreement with the Adjust R^2 of 0.9527. The Predicted R^2 = 0.9684 and Adjust R^2 = 0.9527 have almost the same values; the deviation is less than 0.2. Therefore, the SR model is considered adequate and can accurately predict the response in the range of burnishing conditions used. For the SR model, the single terms (S, D, and f) and the quadratic terms (S^2, D^2, and f^2) are named as the significant factors. The contributions of the S, D, and f are 37.12%, 25.40%, and 27.35%, respectively. The contributions of the S^2, D^2, and f^2 are 3.91%, 1.24%, and 4.69%, respectively (Fig. 5a).

Table 4. ANOVA results for the SR model

Source	Sum of Squares	Mean Square	F-Value	p-value	Remark	Contributions (%)
Model	0.5076	0.0564	31.33	< 0.0001	Significant	
S	0.1900	0.1900	105.56	< 0.0001	Significant	37.12
D	0.1300	0.1300	72.22	< 0.0001	Significant	25.40
f	0.1400	0.1400	77.78	< 0.0001	Significant	27.35
SD	0.0002	0.0002	0.13	0.6083	Insignificant	0.04
Sf	0.0004	0.0004	0.22	0.4977	Insignificant	0.08
Df	0.0009	0.0009	0.50	0.319	Insignificant	0.18
S^2	0.0200	0.0200	11.11	0.0015	Significant	3.91
D^2	0.0063	0.0063	3.51	0.0249	Significant	1.24
f^2	0.0240	0.0240	13.33	0.0008	Significant	4.69
Residual	0.0124	0.0018				
Cor Total	0.5200					
R^2 = 0.9762; Predicted R^2 = 0.9684; Adjust R^2 = 0.9527						

Table 4 presents ANOVA results for the VH model. We find that "F value" of the model is 38.90, which confirms that it is significant. The level of significance is 0.05, which is a confidence level of 95%. R^2 of 0.9804 is in reasonable agreement with the Adjust R^2 of 0.9582. The Predicted R^2 = 0.9724 and Adjust R^2 = 0.9582 have almost the same values; the deviation is less than 0.2. Therefore, the VH model is considered adequate and can accurately predict the response in the range of burnishing conditions used. For the VH model, the single terms (S, D, and f), the interactive term (Sf and Df), and the quadratic terms (S^2, D^2, and f^2) are named as the significant factors. The contributions of the S, D, and f are 21.16%, 33.30%, and 27.29%, respectively. The contirbutions of the Sf and Df are 2.62% and 1.52%, respectively. The contributions of the S^2, D^2, and f^2 are 3.48%, 4.84%, and 5.56%, respectively (Fig. 5b).

Comparisons of the predicted and actual values for the SR and VH models are shown in Figs. 6a and b, respectively. The fact that the data are consistently distributed along straight lines suggests that the generated correlations are adequate.

Table 5. ANOVA results for the VH model

Source	Sum of Squares	Mean Square	F-Value	p-value	Remark	Contributions (%)
Model	2994.42	332.71	38.90	< 0.0001	Significant	
S	639.03	639.03	74.72	< 0.0001	Significant	21.16
D	1005.76	1005.76	117.61	< 0.0001	Significant	33.30
f	824.18	824.18	96.37	< 0.0001	Significant	27.29
SD	6.5	6.50	0.76	0.0868	Insignificant	0.22
Sf	79.21	79.21	9.26	0.0002	Significant	2.62
Df	46.01	46.01	5.38	0.0004	Significant	1.52
S^2	104.95	104.95	12.27	< 0.0001	Significant	3.48
D^2	146.2	146.20	17.10	< 0.0001	Significant	4.84
f^2	168.05	168.05	19.65	< 0.0001	Significant	5.56
Residual	59.86	8.55	353.12			
Cor Total	3054.28					
R^2	0.9804					

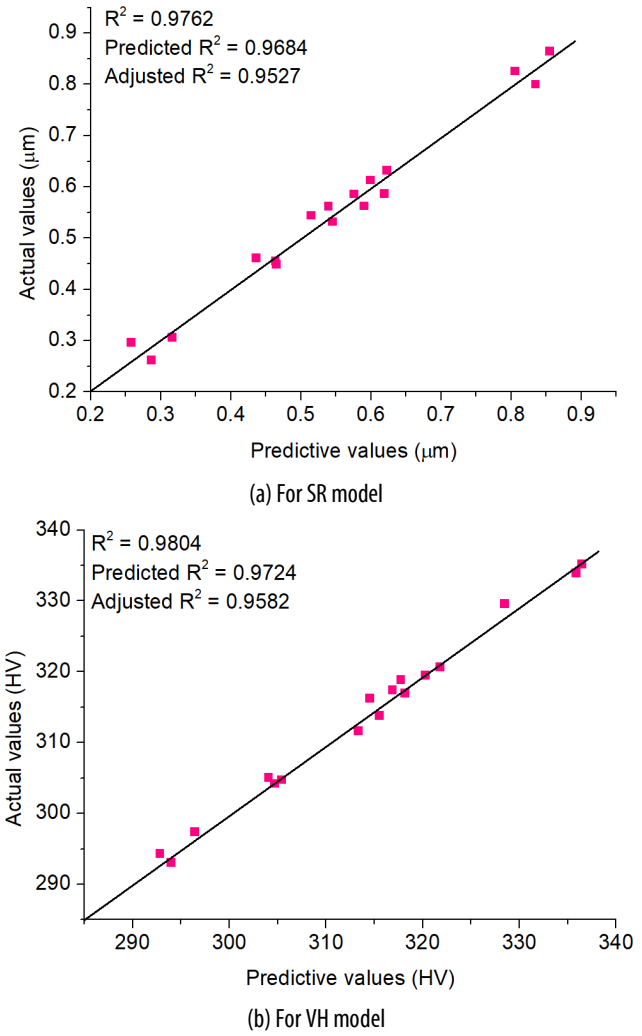

(a) For SR model

(b) For VH model

Fig. 6. Comparisons between the predictive and actual values for burnishing responses

4.3. Impacts of process parameters on burnishing responses

The effects of process factors on the SR are shown in Fig. 7. It is preferable to have low surface roughness to improve the quality of machining.

The effect of the S on the SR is shown in Fig. 7a. Consequently, an increased S results in a lower roughness. The temperature in the burnishing area rises with an increased spindle speed; as a result, the workpiece's strength and hardness diminish. There is a noticeable decrease in roughness and the material compresses readily.

The effect of the D on the SR is shown in Fig. 7b. A tiny quantity of material is crushed and the machining pressure is reduced when the burnishing depth is minimal. There is less plastic deformation, which results in increased roughness. A greater degree of plastic deformation is produced by a higher machining pressure that results from an increased burnishing depth. Low roughness and increased material compression are achieved.

The effect of the D on the SR is shown in Fig. 7b. A tiny quantity of material is crushed and the machining pressure is reduced when the burnishing depth is minimal. There is less plastic deformation, which results in increased roughness. A greater degree of plastic deformation is produced by a higher machining pressure that results from an increased burnishing depth. Low roughness and increased material compression are achieved.

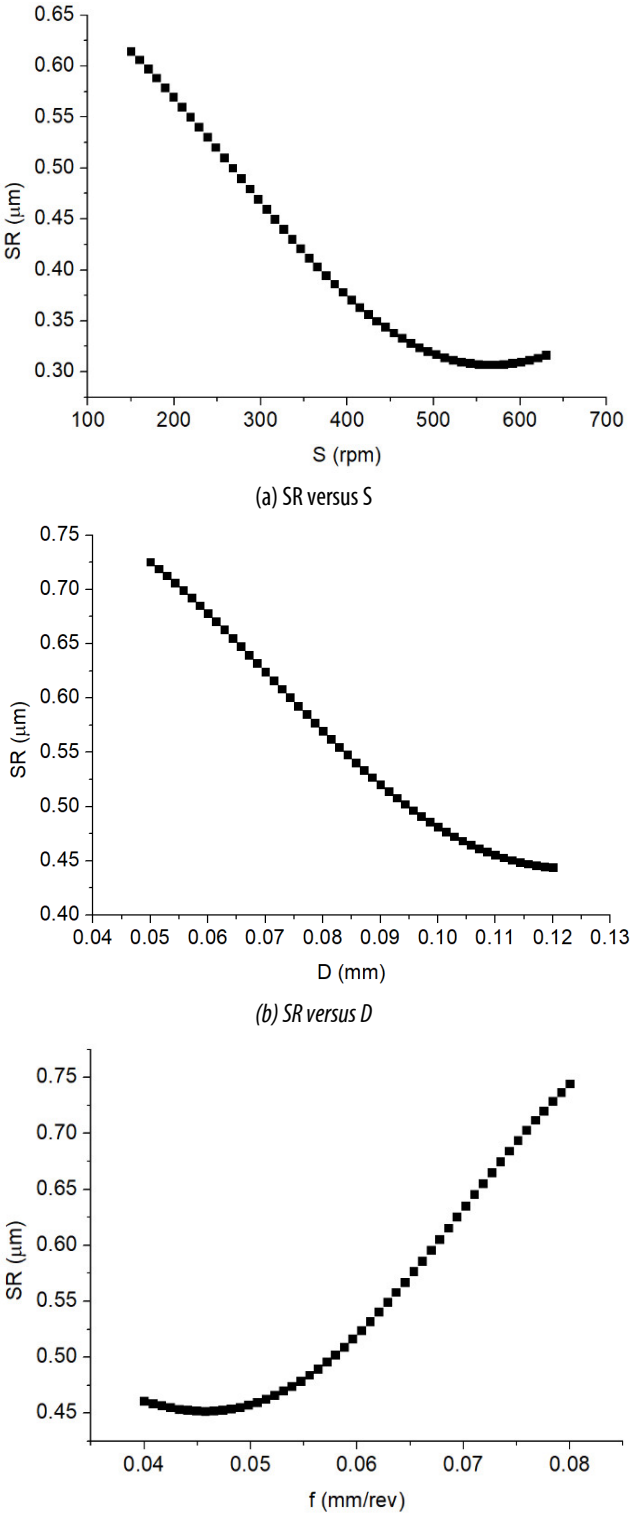

(a) SR versus S

(b) SR versus D

(c) SR versus f

Fig. 7. The main impacts of process parameters on the SR

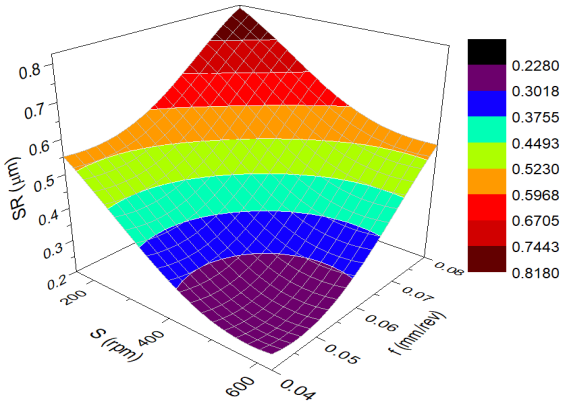

(a) SR versus S and f

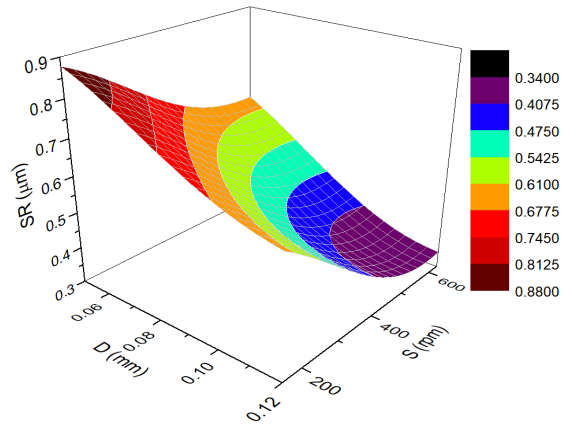

(b) SR versus S and D

Fig. 8. Interactive impacts of process parameters on the SR

The interactive impacts of the process parameters on the SR are shown in Fig. 8.

Fig. 9 presents the influences of the process parameters on the VH. High Vickers hardness is desirable to enhance the machining quality.

As shown in Fig. 9a, the VH decreases with an increased S. A higher S increases the engagement frequency, leading to more burnishing traces on the machined surface. A higher burnishing temperature is generated, leading to a lower hardness.

A higher D results in an increase in VH, as Fig. 9b illustrates. A greater D results in a higher machining pressure, which softly compresses the material and raises the VH. Furthermore, a higher D raises the machining temperature and causes the workpiece surface to exhibit work-hardening behavior, which raises the VH.

Fig. 9c illustrates how the VH decreases with a higher f. Because there is more space between successive traces when f is higher, there is less plastic deformation, which results in a drop in the VH. Furthermore, a greater f shortens the time needed to compress the material during burnishing; as a result, the burnishing tool's impact lessens, lowering the VH.

The interactive impacts of the process parameters on the VH are shown in Fig. 10.

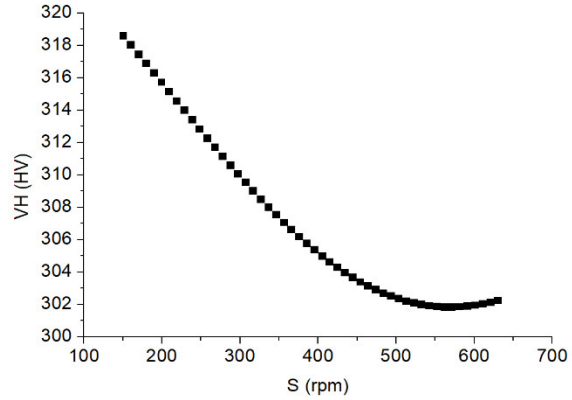

(a) VH versus S

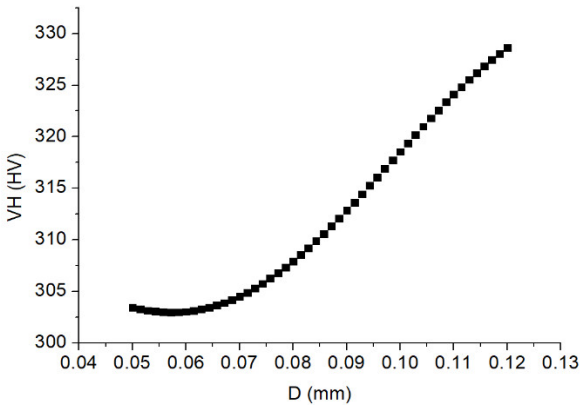

(b) VH versus D

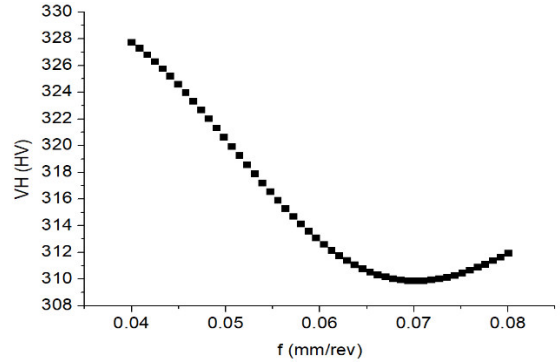

(c) VH versus f

Fig. 9. The main impacts of process parameters on the VH

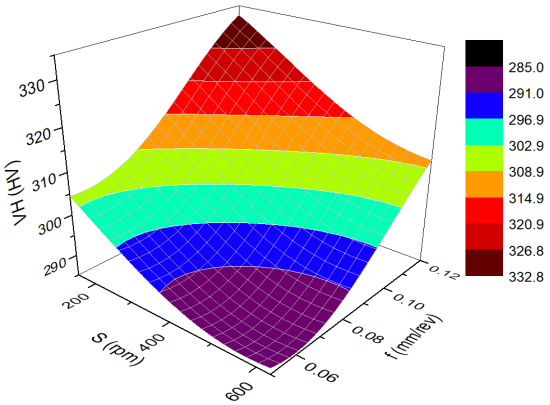

(a) VH versus S and f

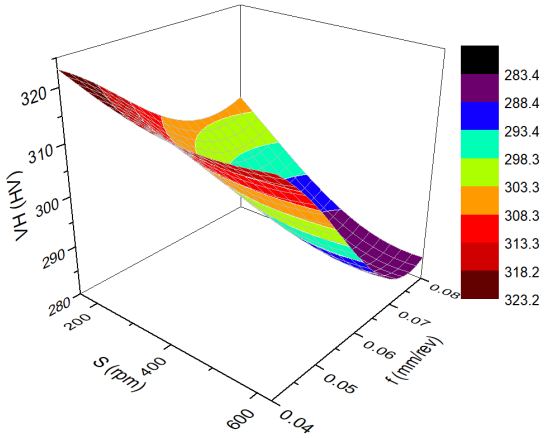

(b) VH versus S and D

Fig. 10. Interactive impacts of process parameters on the VH

4.4. Optimal outcomes produced by the MOPSO

Table 6 lists the entropy, dispersion, and weight values for the technical responses. As a result, the weight values of the SR and VH are 0.51 and 0.49, respectively.

Table 6. Entropy value, dispersion value, and weight for each criterion

Criteria	*SR*	*VH*
Entropy value	0.1098	0.1347
Dispersion value	0.8902	0.8653
Weight	0.51	0.49

Fig. 11 shows the Pareto graphs produced by MOPSO. Consequently, a low VH causes a reduction in the SR. As a results, the best results produced by the S, D, and f are 630rpm, 0.012mm, and 0.04mm/rev, respectively. At the selected solution, the VH is improved by 10.2%, while the SR is down 60.9% (Table 7).

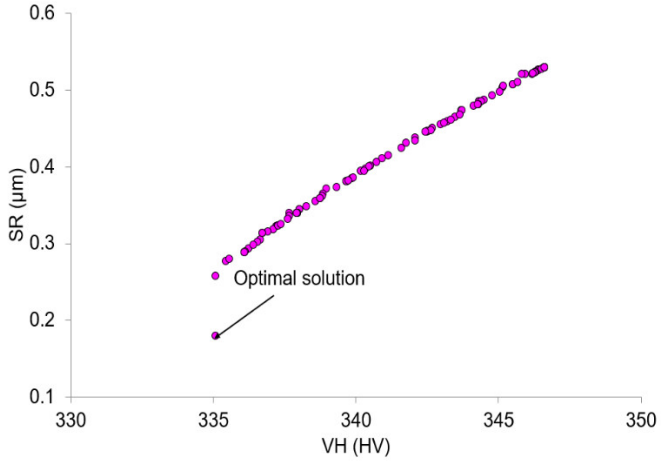

Fig. 11. Pareto fronts generated by MOPSO

Table 7. Optimization results produced by the MOPSO

Method	S (RPM)	D (mm)	f (mm/rev)	SR (µm)	VH (HV)
Initial results	370	0.08	0.06	0.46	304.2
Optimal results	630	0.12	0.04	0.18	335.2
Improvements (%)				-60.9	10.2

At the selected solution, the SR is reduced by 95.1%, while the VH is improved by 59.0%, as compared to the pre-burnished conditions. The SEM image of the burnished surface at the optimal point is presented in Fig. 12. The roughness profile at the selected solution is shown in Fig. 13. It can be stated that the peaks and valleys were comprehensively flattened and filled with the aid of the diamond burnishing operation.

Table 8. Comparisons between pre-burnished and burnished surface

Surface characteristics	SR (µm)	VH (HV)
Pre-burnished	3.68	210.8
Burnished surface	0.18	335.2
Improvements (%)	95.1	-59.0

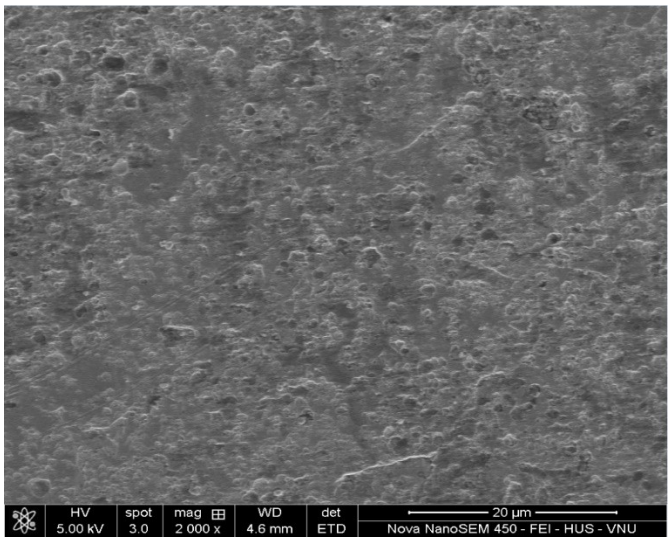

Fig. 12. The SEM image of the burnished surface

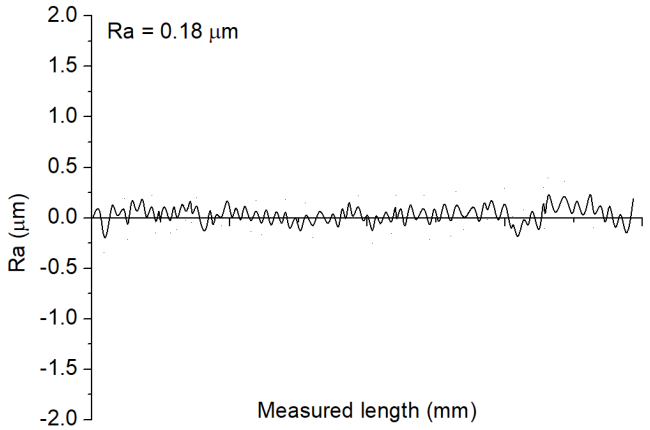

Fig. 13. The roughness profile of the burnished surface

5. CONCLUSION

To improve the surface quality, a novel diamond burnishing procedure utilizing the Vortex tube and liquid CO_2 was created in this study. The ideal values of the S, D, and f were used to achieve the improvements in the SR and VH. The process parameters were taken into consideration when developing the ANN models for the burnishing

reactions. To calculate the weights and identify the best results, the entropy technique and MOPSO were applied. The findings can be stated as follows:

1. It can be said that the burnishing responses are significantly influenced by process factors. The maximum spindle speed and burnishing depth might be used to reduce the surface roughness, however a low feed rate was advised. Using the maximum burnishing depth and the lowest spindle speed and feed rate would increase Vickers hardness.

2. The spindle speed dominated the SR model, with feed rate and burnishing depth coming in second and third, respectively. The burnishing depth was found to be the most important parameter for the VH model, with feed rate and spindle speed coming in second and third, respectively.

3. The optimal parameters the S, D, and f were 630rpm, 0.12mm, and 0.04mm/rev., respectively. The SR was decreased by 60.9%, while the VH was increased by 10.2% at the optimal solution.

4. The Vortex tube and liquid CO_2 in a new lubrication system could improve the cooling effectiveness of other machining operations. The discovered results can be used in industrial settings to reduce the need for human labor, save the cost of experiments, and improve burnishing quality.

5. The ANN and MOPSO could be utilized to determine the optimal process parameters for other machining operations.

6. The developed diamond tool could be used to produce other internal holes.

7. The energy efficiency and product costs will be explored in future works.

REFERENCES

[1]. Maximov J. T., Duncheva G. V., Anchev A. P., Ganev N., Amudjev I. M., Dunchev V. P., "Effect of slide burnishing method on the surface integrity of AISI 316Ti chromium-nickel steel," *J. Braz. Soc. Mech. Sci. Eng.,* 40: 194, 2018.

[2]. Maximov J. T., Duncheva G. V., Anchev A. P., Dunchev V. P., Ichkova M. D., "Improvement in fatigue strength of 41Cr4 steel through slide diamond burnishing," *J. Braz. Soc. Mech. Sci. Eng.,* 42: 197, 2020.

[3]. Maximov J. T., Duncheva G. V., Anchev A. P., Dunchev V. P., "Smoothing, deep, or mixed diamond burnishing of lowalloy steel components - optimization procedures," *Int. J. Adv. Manuf. Technol.*, 106: 1917-1929, 2020.

[4]. Korzynski M., Dudek K., Palczak A., Kruczek B., Kocurek P., "Experimental models and correlations between surface parameters after slide diamond burnishing," *Meas. Sci. Rev.*, 18: 123-129, 2018.

[5]. Kluz R., Antosz K., Trzepieciński T., Bucior M., "Modelling the influence of slide burnishing parameters on the surface roughness of shafts made of 42CrMo4 heat-treatable steel," *Materials*, 14: 1175, 2021.

[6]. Sachin B., Narendranath S., Chakradhar D., "Application of Desirability Approach to Optimize the Control Factors in Cryogenic Diamond Burnishing," *Arab. J. Sci. Eng.*, 45: 1305-1317, 2020.

[7]. Zaghal J., Molnár V., Benke M., "Improving surface integrity by optimizing slide diamond burnishing parameters after hard turning of 42CrMo4 steel," *Int. J. Adv. Manuf. Technol.*, 128: 2087-2103, 2023.

[8]. Felhő C., Varga G., "CAD and FEM Modelling of Theoretical Roughness in Diamond Burnishing," *Int. J. Precis. Eng. Manuf.*, 23: 375-384, 2022.

[9]. Galya V. Duncheva, Jordan T. Maximov, Angel P. Anchev, Vladimir P. Dunchev, Yaroslav B. Argirov, "Multi-objective optimization of the internal diamond burnishing process," *Mater. Manuf. Process.*, 37(4): 428-436, 2022.

[10]. Yilmazkaya E. "Amperage prediction in mono-wire cutting operation using multiple regression and artificial neural network models," *Neural Comput & Applic*, 35: 13343-13358, 2023.

[11]. Zhang J., Xiang X., Zhang Q., et al., "Particle swarm optimization-based subsea cable electromagnetic detection by autonomous underwater vehicle," *Neural Comput & Applic*, 2023. DOI: 10.1007/s00521-023-09060-4.